Article

Theoretical Analysis of the Influence of Pore Geometry on Monomolecular Cracking and Dehydrogenation of n-Butane in Brønsted-Acid Zeolites

Jeroen Van der Mynsbrugge, Amber Janda, Shaama Mallikarjun Sharada, Li-Chiang Lin, Veronique Van Speybroeck, Martin Head-Gordon, and Alexis T. Bell

ACS Catal., **Just Accepted Manuscript** • DOI: 10.1021/acscatal.6b03646 • Publication Date (Web): 01 Mar 2017

Theoretical Analysis of the Influence of Pore Geometry on Monomolecular Cracking and Dehydrogenation of n-Butane in Brønsted-Acidic Zeolites

Jeroen Van der Mynsbrugge,[1,3] Amber Janda,[1†] Shaama Mallikarjun Sharada,[1‡] Li-Chiang Lin,[4] Veronique Van Speybroeck,[3] Martin Head-Gordon,[2] and Alexis T. Bell[1]*

[1]Department of Chemical and Biomolecular Engineering
University of California, Berkeley, CA 94720, USA

[2]Department of Chemistry
University of California, Berkeley, CA 94720, USA

[3]Center for Molecular Modeling
Ghent University
Tech Lane Ghent Science Park Campus A, Technologiepark 903
9052 Zwijnaarde, Belgium

[4]William G. Lowrie Department of Chemical and Biomolecular Engineering
The Ohio State University
151 W. Woodruff Ave.
Columbus, OH 43210, USA

Submitted to

ACS Catalysis
(Date)

*To whom correspondence should be addressed: alexbell@berkeley.edu

Present address:
† A. J.: Department of Chemical Engineering, Stanford University, Stanford, CA 94305, USA
‡ S. M. S.: (1) SUNCAT Center for Interface Science and Catalysis, SLAC National Accelerator Laboratory, Menlo Park, CA 94025, USA; (2) Department of Chemical Engineering, Stanford University, Stanford, CA 94305, USA

Abstract

Recent experimental work has shown that variations in the confinement of n-butane at Brønsted-acid sites due to changes in zeolite framework structure strongly affect the apparent and intrinsic enthalpy and entropy of activation for cracking and dehydrogenation. Quantum chemical calculations have provided good estimates of the intrinsic enthalpies and entropies of activation extracted from experimental rate data for MFI, but extending these calculations to less confining zeolites has proven challenging, particularly for activation entropies. Herein, we report our efforts to develop a theoretical model for the cracking and dehydrogenation of n-butane occurring in a series of zeolites containing 10-membered ring channels and differing in cavity size (TON, FER, -SVR, MFI, MEL, STF and MWW). We combine a QM/MM approach to calculate intrinsic and apparent activation parameters, with thermal corrections to the apparent barriers obtained from configurational-bias Monte Carlo simulations, to account for configurational contributions due to global motions of the transition state. We obtain good agreement between theory and experiment for all activation parameters for central cracking. For terminal cracking and dehydrogenation, good agreement between theory and experiment is found only at the highest confinements. Experimental activation parameters, especially those for dehydrogenation, tend to increase with decreasing confinement. This trend is not captured by the theoretical calculations, such that deviations between theory and experiment increase as confinement decreases. We propose that because transition states for dehydrogenation are later than those for cracking, relative movements between the fragments produced in the reaction become increasingly important in the less confining zeolites.

Keywords (5-8)

zeolites, confinement, QM/MM, CBMC, chemical kinetics, apparent rate parameters, activation enthalpy, activation entropy

1 Introduction

Brønsted-acidic zeolites are used extensively in petroleum refining to crack alkanes (C_nH_{2n+2}) into lower molecular weight alkanes and alkenes (C_mH_{2m+2} and $C_{n-m}H_{2(n-m)}$). At very low alkane conversion, the Brønsted-acid sites are mostly unoccupied and cracking, as well as dehydrogenation (which produces C_nH_{2n} and H_2) occur by a monomolecular mechanism involving a direct activation of the alkane by the zeolite proton.[1-6] The kinetics of both monomolecular processes are first-order in alkane.[7-9] Moreover, because alkane molecules are activated directly by protons in the rate-determining step, kinetic parameters determined from the apparent rate coefficient, k_{app}, can be used to interpret the intrinsic effects of the active site environment on catalysis. Therefore, monomolecular reactions of alkanes are useful probe reactions for characterizing the influence of zeolite structure on kinetics.

In recent experimental studies, we have shown that the apparent and intrinsic first-order rate coefficients (k_{app} and k_{int}) and the apparent and intrinsic enthalpy and entropy of activation ($\Delta H^{\ddagger}_{app}$ and $\Delta S^{\ddagger}_{app}$, $\Delta H^{\ddagger}_{int}$ and $\Delta S^{\ddagger}_{int}$) for central and terminal cracking and for dehydrogenation of n-butane are sensitive to the extent of reactant confinement described by the entropy of n-butane adsorption at Brønsted-acid sites ($\Delta S_{ads\text{-}H+}$).[10] To determine values of $\Delta H^{\ddagger}_{int}$ and $\Delta S^{\ddagger}_{int}$, we employed Eqns. 1 and 2, which follow directly from the rate expression for monomolecular cracking and dehydrogenation[10,11]:

(1) $$\Delta H^{\ddagger}_{app} = \Delta H_{ads\text{-}H+} + \Delta H^{\ddagger}_{int}$$

(2) $$\Delta S^{\ddagger}_{app} = \Delta S_{ads\text{-}H+} + \Delta S^{\ddagger}_{int}$$

In these equations, $\Delta H_{ads\text{-}H+}$ and $\Delta S_{ads\text{-}H+}$ are the enthalpy and entropy of adsorption of the alkane at a Brønsted-acid site and are determined using configurational-bias Monte Carlo (CBMC) simulations because experimental adsorption measurements are not possible at temperatures

corresponding to reaction conditions (> 673 K).[10,11] Values of $\Delta H^{\ddagger}_{int}$ and $\Delta S^{\ddagger}_{int}$ can be determined by subtracting values of $\Delta H_{ads\text{-}H+}$ and $\Delta S_{ads\text{-}H+}$ from $\Delta H^{\ddagger}_{app}$ and $\Delta S^{\ddagger}_{app}$, which are extracted directly from measured rate data and are referenced to the gas phase. The relation between apparent and intrinsic activation parameters is illustrated in Figure 1.

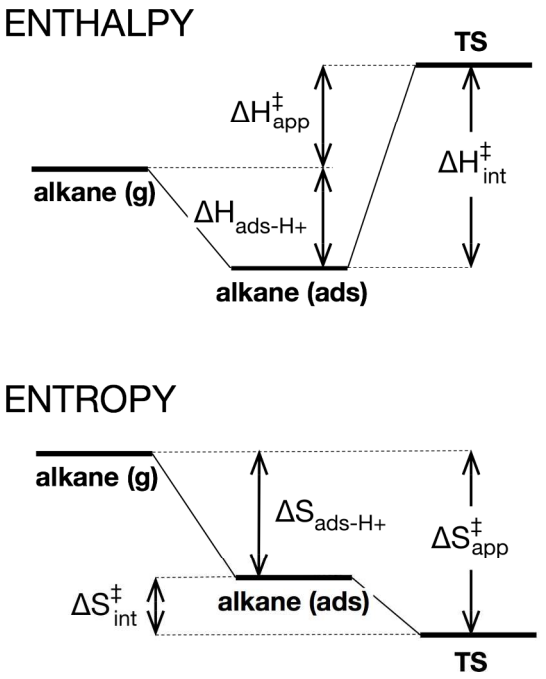

Figure 1. Schematic enthalpy and entropy landscapes for monomolecular alkane cracking or dehydrogenation over Brønsted-acid zeolites. The adsorption enthalpy ($\Delta H_{ads\text{-}H+}$) and adsorption entropy ($\Delta S_{ads\text{-}H+}$) of the alkane at a Brønsted-acid site is determined using configurational-bias Monte Carlo (CBMC) simulations.[10,11] Intrinsic activation parameters ($\Delta H^{\ddagger}_{int}$ and $\Delta S^{\ddagger}_{int}$) are determined by subtracting $\Delta H_{ads\text{-}H+}$ and $\Delta S_{ads\text{-}H+}$ from apparent parameters ($\Delta H^{\ddagger}_{app}$ and $\Delta S^{\ddagger}_{app}$) extracted directly from measured rate data.

We have found that the resulting values of $\Delta H^{\ddagger}_{int}$ and $\Delta S^{\ddagger}_{int}$ depend on the zeolite framework for n-butane,[10] as well as for n-hexane using previously reported rate data.[12] For n-butane, more confining zeolites (as inferred by more negative values of $\Delta S_{ads\text{-}H+}$) exhibited lower values of $\Delta H^{\ddagger}_{int}$ and $\Delta S^{\ddagger}_{int}$ for terminal cracking and for dehydrogenation, while values for central cracking are not strongly dependent on confinement.[10] (For n-hexane, values of $\Delta H^{\ddagger}_{int}$

and $\Delta S^{\ddagger}_{int}$ corresponded to ensemble averages over all reaction paths, as selectivity data were not reported in the original study.[10,12]) The differing dependence of activation parameters corresponding to different reaction pathways on confinement was attributed to the position of each transition state along its respective reaction coordinate, with $\Delta H^{\ddagger}_{int}$ and $\Delta S^{\ddagger}_{int}$ for later transition states (e.g., dehydrogenation) exhibiting a higher sensitivity to confinement.

These findings represent the first report, to our knowledge, that the zeolite structure can affect the values of $\Delta H^{\ddagger}_{int}$ and $\Delta S^{\ddagger}_{int}$ because of differences in confinement. Although Gounder and Iglesia[13] have described the transition state for propane dehydrogenation as being later than that of cracking based on transition-state structures obtained from density functional theory,[14] these authors concluded that $\Delta H^{\ddagger}_{int}$ and $\Delta S^{\ddagger}_{int}$ do not vary with the structural environment of Brønsted-acidic protons based on arguments that a change in confinement affects the stabilization of reactant and transition states to the same extent, and that a high charge density on the transition state prevents confinement from affecting $\Delta S^{\ddagger}_{int}$.[15] In fact, prior to our recent work,[10] the consensus in the literature has been that $\Delta H^{\ddagger}_{int}$[12,13,16-18] and $\Delta S^{\ddagger}_{int}$[12,15,16] are independent of zeolite framework type and that $\Delta H^{\ddagger}_{int}$ is affected only by the "acidity" of the Brønsted protons. However, these conclusions were based on experimental results for a more limited number of zeolites relative to ref. 10 and on values of $\Delta H^{\ddagger}_{int}$ and $\Delta S^{\ddagger}_{int}$ that were estimated using Eqns. 1 and 2 together with values of $\Delta H_{ads\text{-}H+}$ and $\Delta S_{ads\text{-}H+}$ measured near ambient temperature (which reduces the accuracy of $\Delta H^{\ddagger}_{int}$ and $\Delta S^{\ddagger}_{int}$).[11] The recent findings of ref. 10, therefore, suggest that a theoretical investigation of the effects of zeolite structure on activation enthalpies and entropies for alkane monomolecular reactions is needed to better understand how confinement influences these processes.

Several theoretical studies of n-alkane monomolecular cracking and dehydrogenation have been reported previously.[3-6,11,14,19-31] Most of these investigations have focused on determining activation energies, and good agreement between electronic structure theory and experiment was reported for a limited set of zeolites. Several studies have also reported free energies or entropies of activation.[3,5,6,11,23,24,32] Good agreement between theory and experiment has been reported for $\Delta S^{\ddagger}_{int}$ for alkane cracking in MFI using a composite hindered rotor approach adapted from that reported by Grimme[33] to account for internal rotations.[11] However, no previous studies have attempted to describe the activation entropy for dehydrogenation. Positive values of $\Delta S^{\ddagger}_{int}$ for dehydrogenation have been determined experimentally,[10,13,34] but have not been interpreted in theoretical studies.

We also note that theoretical investigations of the effects of active site environment on kinetics have been very limited. While a few studies have investigated the effects of induced changes in acidity,[14,24,29] only three of the abovementioned studies have investigated the effects of structural confinement.[5,20,22] Sharada et al. have reported that activation energies for n-butane cracking and dehydrogenation differ for intersection and sinusoidal channel sites of MFI.[20] Bučko et al. have investigated the effect of channel environment within MOR on the intrinsic activation parameters for propane cracking using ab initio molecular dynamics simulations and transition path sampling.[5] These authors reported that the activation entropy is less negative for 8-ring vs. 12-ring pores due to the smaller loss of entropy between the reactant and transition state in more confining locations. The same interpretation was used to explain the decrease in the experimental value of $\Delta S^{\ddagger}_{int}$ with decreasing confinement observed for n-butane central cracking in ref. 10. Maihom et al. have used density functional theory to investigate n-hexane activation within MFI and FAU.[22] They showed that the intrinsic activation energy for cracking at the

centermost C-C bond is nearly the same for MFI and FAU, consistent with the invariance of the experimental value of $\Delta H^{\ddagger}_{int}$ for n-butane central cracking with respect to confinement observed in ref. 10. Other reaction pathways for n-hexane cracking, such as terminal C-C cracking and dehydrogenation (those for which activation parameters were found to vary with confinement for n-butane in ref. 10), were not investigated by Maihom et al.[22]

The above discussion shows that a complete understanding of the influence of reactant and transition state confinement near the zeolite Brønsted-acid center on the kinetics of monomolecular alkane activation is lacking. The aim of the present study is to carry out a theoretical analysis of how the shape and size of zeolite pores affect the apparent and intrinsic enthalpies and entropies of activation for butane cracking and dehydrogenation. A previously applied QM/MM approach[20] is supplemented with thermal corrections, derived from CBMC simulations of n-butane adsorbed in the reactant state,[10] to include configurational effects at low computational cost. Inclusion of these corrections results in good quantitative agreement between theoretically predicted and experimentally determined values of $\Delta H^{\ddagger}_{app}$ and $\Delta S^{\ddagger}_{app}$ for central cracking of butane in all zeolites. Calculated values of $\Delta H^{\ddagger}_{int}$ and $\Delta S^{\ddagger}_{int}$, which do not include configurational corrections, also agree well with experimentally measured values for central cracking. For terminal cracking and dehydrogenation of butane, the agreement of both apparent and intrinsic activation parameters between theory and experiment is good for zeolites with the most confining structures. As the confinement decreases, theory underestimates the experimental values of $\Delta H^{\ddagger}_{app}$ and $\Delta H^{\ddagger}_{int}$ and (more strongly) the values of $\Delta S^{\ddagger}_{app}$ and $\Delta S^{\ddagger}_{int}$, which increase with decreasing confinement. This deviation is much more significant for dehydrogenation than for terminal cracking and is attributed to the fact that terminal cracking and particularly dehydrogenation occur via transition states that are later than that for central cracking. The

deviation of theoretical and experimental activation parameters at low confinement is very likely due to the failure of the theoretical methods to account for the non-correlated rotations and translations of the product-like fragments making up late transition state structures.

2 Theoretical Methods

2.1 Zeolite models

Seven zeolites were chosen for theoretical analysis. These zeolites (TON, FER, -SVR, MFI, MEL, STF and MWW) feature 10-ring channels and are appropriate for a study of the effects of confinement on monomolecular reaction kinetics because they represent a wide range of confinements for Brønsted-acid sites. The level of confinement for each zeolite within a given channel topology (e.g. straight vs sinusoidal channels) is described by the entropy of adsorption of n-butane adsorbed at an active site, Boltzmann averaged over all T-sites ($\Delta S_{ads\text{-}H+}$).[10] Values of $\Delta S_{ads\text{-}H+}$ for each zeolite can be found in ref. 10.

The crystallographic structures of the zeolites were taken from the database maintained by the International Zeolite Association (IZA),[35] and a single Al atom was introduced into each framework to create the Brønsted acid site required for catalysis. Experimental studies have shown that Al atoms are distributed among crystallographically distinct T-sites and that the distribution of Al in the framework is controlled by the Si/Al ratio and the conditions used for zeolite synthesis.[34,36] Consequently, to appropriately compare the rate parameters determined from experiments with those predicted by theory, one should Boltzmann-average the predicted values obtained for different Al sites within each zeolite. Since this approach would be very resource-intensive, QM/MM calculations for each zeolite structure were carried out for

representative T-sites chosen as discussed below, to sample the widest possible range of structural environments while also considering the tendency of the adsorbed alkane to locate within less confining spaces (e.g. cages, if present, rather than channels) at reaction temperatures.[11] Selection of T-sites in this way ensures that changes in confinement occur for reactant and transition states (TS) in moving from zeolites with higher average confinement (i.e., lower values of $\Delta S_{ads\text{-}H+}$) to those with lower overall confinement (i.e., higher values of $\Delta S_{ads\text{-}H+}$). A further advantage of our approach is that it allows us to focus on distinctive cavities within each of the zeolite frameworks and to be more effective in elucidating the experimentally observed variations in activation parameters among the different zeolites.

For the QM/MM calculations, large clusters were constructed for each of the zeolites to represent the active site and the salient features of its surroundings. These clusters, along with the number of tetrahedral atoms (T-atoms) included in each, are shown in Figure 2. Visual representations of the pore and channel topologies of these zeolites, generated using the ZEOMICS web tool,[37] can be found in ref. 10.

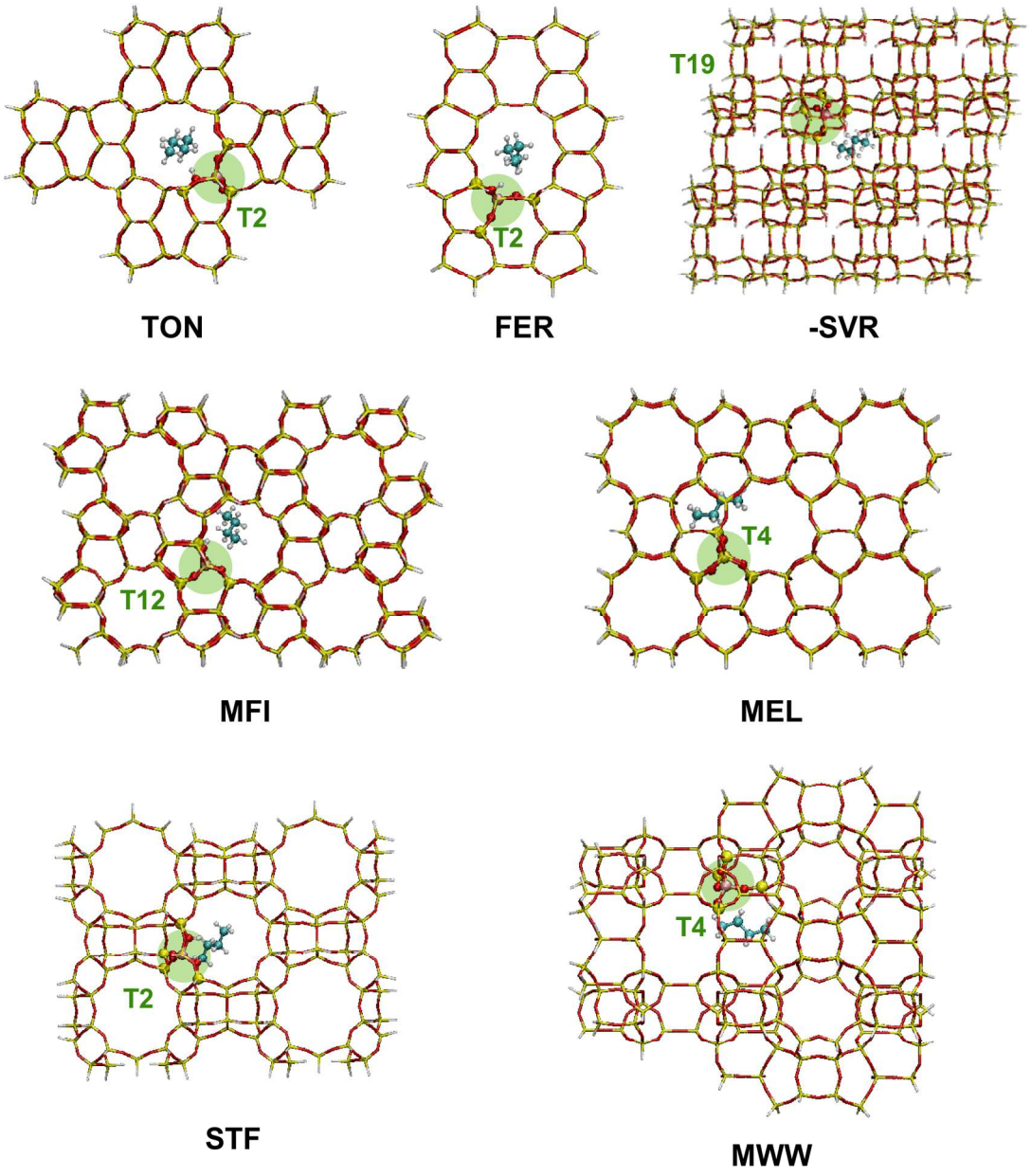

Figure 2. Cluster models used to represent the zeolite catalysts in QM/MM calculations: **TON** (280 T-atom cluster, Al in the T2 site); **FER** (236 T-atom cluster, Al in the T2 site); **-SVR** (348 T-atom cluster, Al in the T19 site); **MFI** (437 T-atom cluster, Al in the T12 site); **MEL** (264 T-atom cluster, Al in the T4 site); **STF** (398 T-atom cluster, Al in the T2 site); **MWW** (292 T-atom cluster, Al in the T4 site). The QM region is depicted using a ball-and-stick representation. Si atoms are shown in yellow, O in red, Al in pink, C in cyan and H in white.

The cluster representations of the seven zeolites presented in Figure 2 can be divided into three groups. The first group comprises three frameworks with straight or sinusoidal channels and no cages, TON, FER and -SVR. In TON, which contains one-dimensional 10-ring straight channels and 4 distinct T-sites, the Al atom was located at the T2 site, based on siting probabilities estimated in a combined NMR and QM/MM study.[38] The -SVR framework has a three-dimensional channel system, consisting of 10-ring sinusoidal channels and smaller side pockets, and contains four ordered defects per unit cell, owing to Si vacancies that occur during synthesis.[39] All terminal oxygen species surrounding these vacancies were replaced with silanol groups[40] and the Al atom was placed in the T19 position, such that the Brønsted-acidic proton is located in the sinusoidal channel.

The second group comprises two three-dimensional frameworks featuring intersecting channel systems, MFI and MEL. These structures lack large cavities, but do possess channel intersections that (for MFI) are thermodynamically preferred over channel sites for n-butane adsorption at 773 K.[11] Therefore, in MFI the Al was placed in the T12 position, which results in the Brønsted-acidic proton being located at the intersection of the straight and sinusoidal channels. This location offers the most available space to accommodate guest molecules and has been selected in several previous studies.[19,20,41-44] The MEL framework consists of intersecting straight channels that have diameters similar to those of the MFI straight channels, but that form a slightly larger cavity at their intersection.[37,45] The Al atom in MEL was placed in the T4 position, such that the Brønsted-acidic proton is again situated at the channel intersection.

The third group of zeolites includes two frameworks featuring large cages (> 8 Å diameter based on the largest included sphere),[37] STF and MWW. STF consists of one-dimensional 10-ring portals connecting large 18-ring pores that form the cages.[46] The Al was

placed in the T2 position, to create an active site within the cage. MWW consists of two independent pore networks, one made up of 10-ring sinusoidal channels, and the other of 12-ring super cages connected by 10-ring channels.[47] Out of 8 possible distinct T sites, Al was substituted into the T4 position based on the results of computational studies that determined that this site is the most energetically stable one for Al substitution.[48,49] This active site is also accessible from the super cage, which represents the least confining space within MWW.

As noted above, placement of Al within the largest spaces of zeolites with intersecting channels or connecting cages is supported by theoretical studies of alkane adsorption. Ab initio molecular dynamics[50] and CBMC adsorption studies[11] have demonstrated that, although adsorption is favored in narrow pores at lower temperatures owing to energetically favorable dispersion interactions between the framework and adsorbate, large pores are favored entropically, and therefore tend to be the preferred sites for adsorption at reaction temperatures (e.g., > 673 K). To further corroborate our placement of Al in the above specified T-sites for the QM/MM calculations in the current study, we examined the site-specific adsorption equilibrium constants ($K_{ads\text{-}H+}$) from the CBMC simulations performed by Janda et al.[10] to confirm that the formation of a reactant state for butane cracking or dehydrogenation at an active site around the selected T-sites is indeed favorable, provided Al substitution occurs there (cf. Table S1 in the Supporting Information).

2.2 QM/MM calculations

The computational approach adopted in this study is largely similar to that used in our previous studies of alkane cracking and dehydrogenation catalyzed by MFI.[20,34] A five tetrahedral atom (T5) cluster containing the active site and the substrate were treated quantum mechanically (QM), and the remaining framework atoms were treated using molecular mechanics (MM).[21,51] The QM region in each of the zeolite models is highlighted using a ball-and-stick representation in Figure 2. All calculations were performed using a developmental version of Q-Chem 3.2.[52] Initial geometries were constructed with ZEOBUILDER.[53] Geometry optimizations as well as vibrational analyses were carried out using the ωB97X-D functional[54,55] and 6-311G(d,p) basis set to describe the QM region. A CHARMM-type force field was used to describe the MM region.[56-58] For the zeolite Si and O atoms in the MM region, Lennard-Jones parameters and charges were taken from previous work (P2 parameter set).[51] These parameters were chosen such that QM/MM adsorption energies not only match pure QM ωB97X-D/6-31+G**results, but also reproduce experimental trends in alkane adsorption energy with respect to chain length.[51] For the silanol hydroxyl groups in the vacancy sites in -SVR we utilized the same MM charge parameters as for the other frameworks, adjusting the charges on the silanol groups to maintain charge neutrality of the entire cluster, rather than re-optimizing the parameters to reproduce energies calculated using pure QM on large clusters.[21] Lennard-Jones parameters and charges for all non-zeolite atoms were taken from the CHARMM set. Single-point energy refinements on the stationary points were performed using the ωB97X-D/6-311++G(3df,3pd) level of theory for the QM region. Transition state guesses were calculated using the freezing string method (FSM)[41,59] and optimized using the partitioned-rational function optimization (P-RFO) technique.[60]

Transition states for cracking correspond to geometries in which the Brønsted acid proton attacks the central or terminal C-C bond, since the alternative involving attack on one of the carbon atoms in the bond was found to significantly underestimate activation enthalpies, and therefore may not correspond to the true rate-limiting step for cracking.[20] The transition state geometries for central cracking, terminal cracking, methylene dehydrogenation and methyl dehydrogenation in MFI are shown in Figure 3. Apart from minor differences in the critical bond distances (cf., Table S2 in the Supporting Information), the transition state geometries, and therefore the mechanism for each cracking or dehydrogenation pathway remained largely invariant with the zeolite environment.

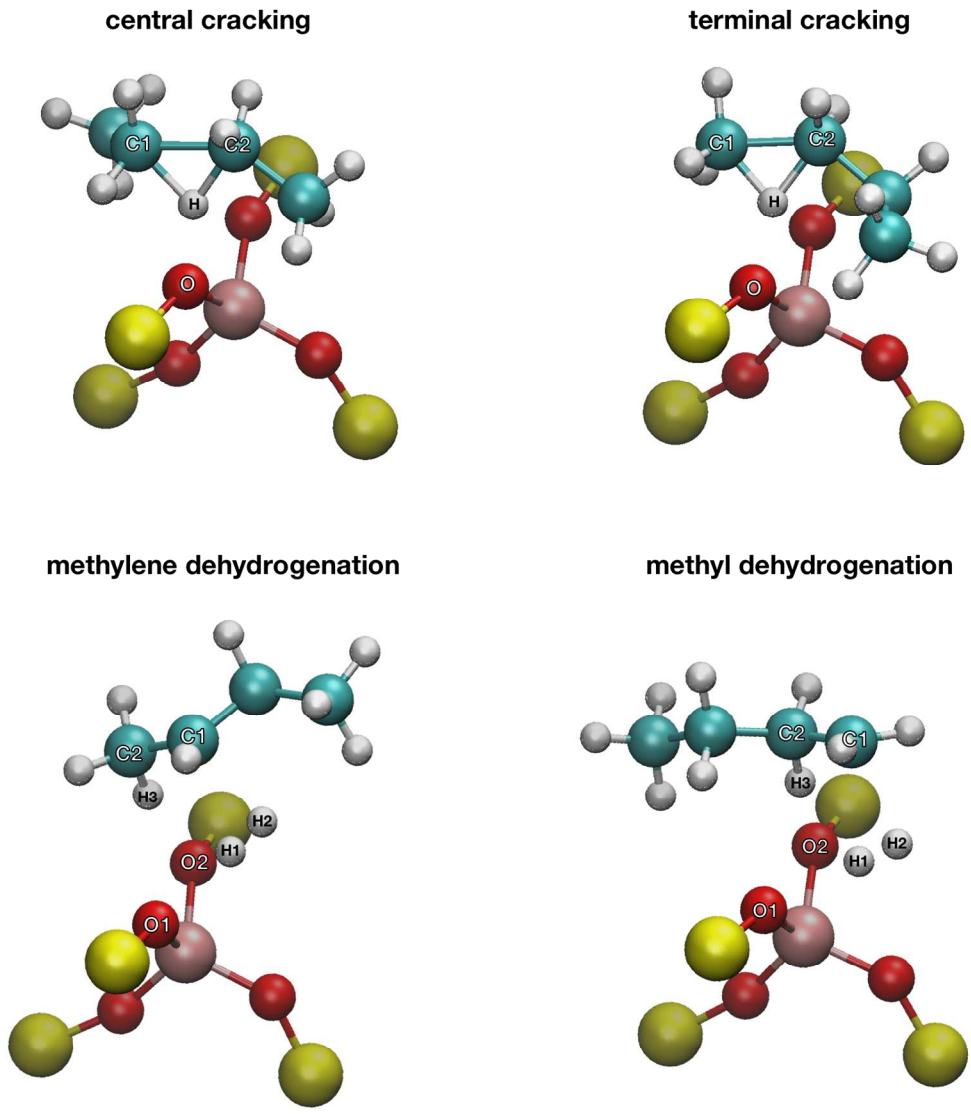

Figure 3. Transition state geometries for central cracking, terminal cracking, methylene dehydrogenation and methyl dehydrogenation in MFI, with Al placed in the T12 site. For clarity, only the atoms included in the QM region are shown. Si atoms are shown in yellow, O in red, Al in pink, C in cyan and H in white.

2.3 Configurational-Bias Monte Carlo (CBMC) simulations

CBMC simulations were carried out to determine the enthalpy and entropy changes for n-butane adsorption onto Brønsted protons (i.e., in a reactant state) from the gas phase. The recently developed one-step approach using the Widom particle insertion method with domain decomposition was employed for this purpose.[10] Non-bonded intra- and inter-molecular interactions are described using the 12-6 Lennard-Jones potential, and each pair-wise interaction is truncated and shifted to zero at a cut-off radius of 12.0 Å. Additionally, bonded interactions (bond stretching, bending, and torsion) are included for modeling n-butane. The potential parameters are taken from our previous work, and have been parameterized to reproduce experimentally measured heats of adsorption for linear C_3-C_6 alkanes in H-FAU.[10] In all simulations, the zeolite framework was treated as a rigid structure with dimensions of at least twice the cut-off radius in all directions. At least 10 million Widom particle insertions were conducted to ensure statistically accurate results.

To better understand the adsorption configurations of n-butane in the reactant state, heat maps (i.e., probability density maps) of the locations of C atoms of butane molecules in a reactant state were generated. To obtain the C atom locations, Monte Carlo simulations in a canonical ensemble (NVT) at infinite dilution (N=1) were performed to collect n-butane configurations every 20 Monte Carlo steps. Each Monte Carlo step represents either a translational move, a rotational move, or a re-insertion move with a probability ratio of 1:1:2, respectively. A total of 4 million configurations were collected from each NVT simulation and C atom locations from more than 16,000 configurations of n-butane were used to generate the heat maps.

2.4 Calculation of enthalpies and entropies of adsorption and activation

Enthalpies and entropies of the reactant and transition states are computed from a normal mode analysis on the various stationary points identified by QM/MM calculations (cf. Section 2.2). The normal mode spectrum of an adsorbed molecule in a zeolite typically includes several low-lying frequencies that correspond to translational and rotational movements of the adsorbate relative to the zeolite framework. Previous studies have shown that treating these modes as vibrations under the rigid rotor-harmonic oscillator (RRHO) approximation typically results in overestimation of the loss in entropy associated with adsorption from the gas phase.[61-63] De Moor et al. have demonstrated that the entropy of hydrocarbons adsorbed inside zeolites cannot be treated within the RRHO approximation and that proper account must be taken of rotational and translational degrees of freedom.[63] These authors performed an analysis based on the Mobile Block Hessian (MBH)[64] method to identify the low-frequency modes that in reality correspond to global translations and rotations of the adsorbate, and found that replacing the corresponding vibrational contributions to the partition function by translational or rotational ones increased the configurational entropy by about 50 J mol^{-1} K^{-1} at 300 K.[63]

The increases in both $\Delta S_{ads\text{-}H+}$ and $\Delta S^{\ddagger}_{int}$ with decreasing confinement observed for dehydrogenation and terminal cracking of n-butane in ref. 10 suggest that the rotational and translational modes described above contribute considerably to the entropies of both reactant and transition-states. While the effects of such global motions, if similar for both states, are expected to largely cancel in calculations of $\Delta S^{\ddagger}_{int}$, (see Eqn. 2), contributions of such modes to $\Delta S^{\ddagger}_{app}$ and $\Delta S_{ads\text{-}H+}$ are expected to be significant. Therefore, to assess the true nature of the low-frequency modes in the reactant and transition states for the cracking and dehydrogenation reactions of interest in this study, we carried out MBH calculations using the TAMKIN package.[65] This

analysis (cf. Section S3 in the Supporting Information) revealed that certain low-lying vibrations in both reactant and transition states are indeed global translations and rotations of the substrate relative to the zeolite framework, indicating that applying the RRHO approximation will also affect the accuracy of apparent entropies of activation.

However, while the mobile block analysis allows unambiguous identification of the vibrational modes to be replaced, the calculation of the corresponding translational entropy performed by De Moor et al. still depends upon an ad hoc estimate of the extent of the translational motion.[63] To avoid this issue, we instead employed a quasi-RRHO approach to mitigate some of the errors in the estimation of thermochemical quantities from vibrational frequencies.[33,51] This method attempts to capture the thermochemical contributions from low-lying modes more accurately by a systematic interpolation between a one-dimensional free rotor at low frequencies and a harmonic oscillator at high frequencies.

We have shown previously that the quasi-RRHO approach to estimate intrinsic activation enthalpies and entropies for central and terminal cracking of n-butane in MFI provides good agreement with experiments.[11] This approach, however, will not be sufficient for determining activation enthalpies and entropies for reactions occurring in zeolites that are less confining than MFI. The reason is that the quasi-RRHO approach relies upon a single geometry (determined using a potential energy surface at 0 K) for both the reactant and transition state, each of which at finite temperature consists of an ensemble of similar structures with slightly different orientations around the active site.[3-5,50,66] Consequently, the entropy (and enthalpy) of the reactant and transition states will be underestimated by quasi-RRHO calculations based on single stationary points (i.e., for the reactant and transition state) with the consequence that apparent activation enthalpies and entropies will also be underestimated. On the other hand, intrinsic

activation entropies will only be underestimated (or overestimated) to the extent that reactant and transition states undergo differing degrees of global translation and rotation.

To overcome this limitation, we derived additional thermal corrections to $\Delta H^{\ddagger}_{app}$ and $\Delta S^{\ddagger}_{app}$ based on CBMC simulations (cf. Section 2.3). If the number of configurations comprising the TS ensemble is assumed to be roughly similar to the number of configurations in the reactant state (butane adsorbed at the Brønsted-acid site), the configurational entropy of the TS can be estimated from the difference between the values of $\Delta S_{ads\text{-}H+}$ at 773 K calculated from QM/MM using the quasi-RRHO approach and those determined from CBMC simulations on butane adsorption at Al in the same T-site, which naturally include contributions from global motions:

(3) $\Delta\Delta S_{config} = \Delta S_{ads\text{-}H+}(\text{CBMC; 773K}) - \Delta S_{ads\text{-}H+}(\text{QM/MM-qRRHO; 773K})$

Following this procedure, the missing configurational entropy in $\Delta S^{\ddagger}_{app}$ for the different reactions is estimated to be 62-86 J mol^{-1} K^{-1}, depending on the zeolite framework (see Table 1). Thermal corrections to $\Delta H^{\ddagger}_{app}$ can be determined in a similar manner. The need for such corrections originates from the fact that higher-enthalpy configurations are accessible at higher temperatures because of the global motions near the active site:

(4) $\Delta\Delta H_{config} = \Delta H_{ads\text{-}H+}(\text{CBMC; 773K}) - \Delta H_{ads\text{-}H+}(\text{QM/MM-qRRHO; 773K})$

Values of $\Delta\Delta H_{config}$ determined using Eqn. 4 are between 10-43 kJ mol^{-1}, depending on the zeolite (Table 1).

Table 1. Thermal corrections to $\Delta H^{\ddagger}_{app}$ and $\Delta S^{\ddagger}_{app}$ for each zeolite framework derived from adsorption thermodynamic data obtained using CBMC simulations at an Al atom in the T-sites used in the QM/MM calculations (in parentheses).

	$\Delta\Delta H_{config}$ kJ mol^{-1}	$\Delta\Delta S_{config}$ J mol^{-1} K^{-1}
TON (T2)	20	62
FER (T2)	10	64
-SVR (T19)	19	69
MFI (T12)	10	75
MEL (T4)	18	81
STF (T2)	11	76
MWW (T4)	43	86

The values of the entropy and enthalpy corrections are highly dependent on the specific characteristics of the zeolite (pore shape and size, location of the active site), as well as the temperature. This point is illustrated in Figure 4, which shows heat maps of the locations of C atoms for butane adsorbed in a reactant state at an Al atom in the T4 site of MWW, obtained from CBMC simulations at different temperatures. In the heat maps, the color indicates the percentage of C atom coordinates found in squares of 0.05 Å by 0.05 Å. Going from a low temperature (50 K) to the reaction temperature (773 K), the region in which butane preferentially adsorbs shifts towards the super cage and becomes significantly more diffuse. These observations demonstrate that, while the single-geometry approximation is valid at very low temperatures, this approximation breaks down at reaction temperatures (> 673 K).[5,50] At elevated temperature, global motions contribute significantly to the enthalpy and, more strongly, to the entropy, and must be considered in calculations of the apparent enthalpies and entropies of butane cracking and dehydrogenation, as discussed below.

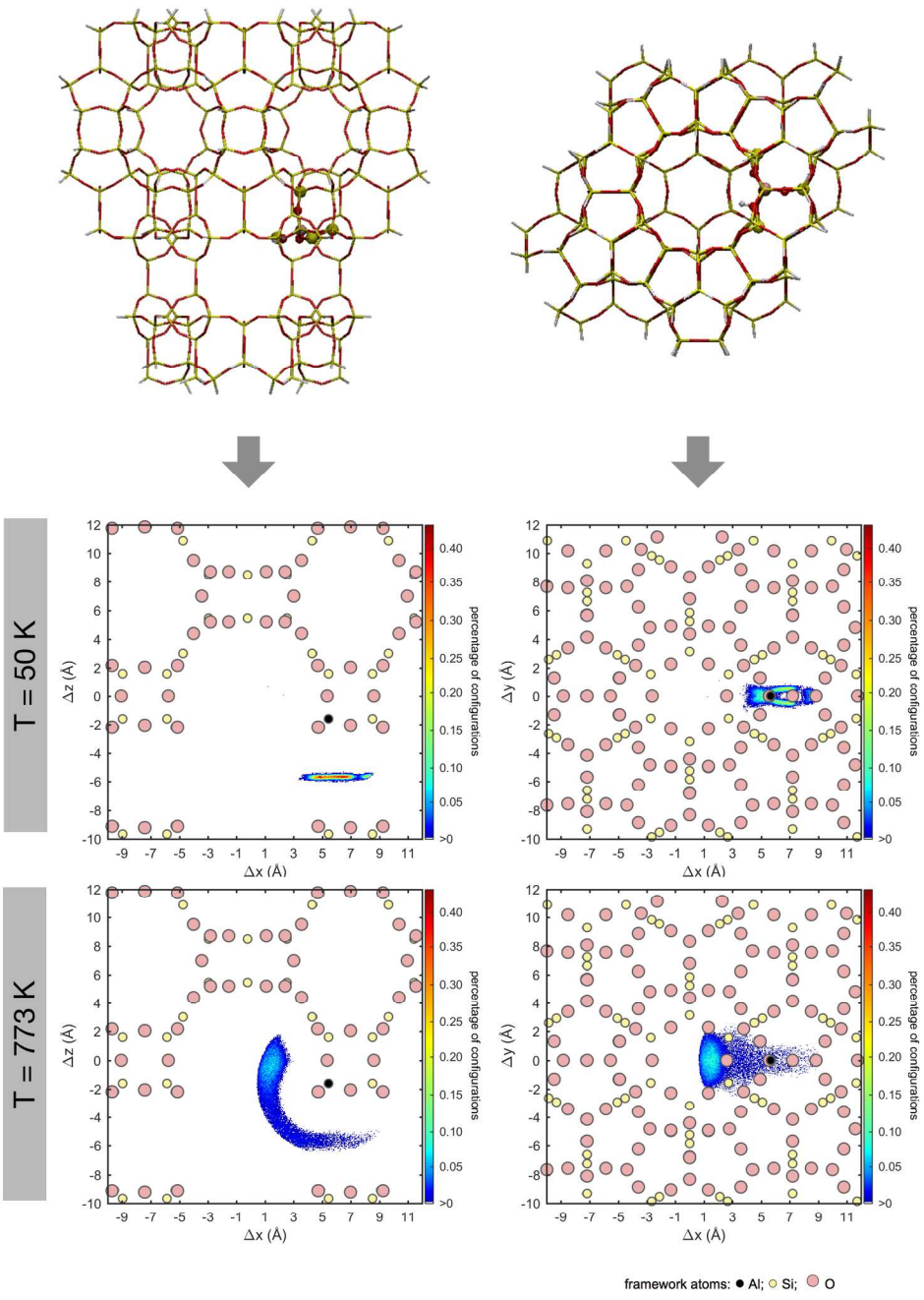

Figure 4. Heat maps showing the distribution of C atoms of the terminal C-C bond for of n-butane interacting via this bond with a Brønsted acid site at site T4 in MWW, obtained from CBMC simulations at 50 K and at 773 K. At 50 K, butane is predominantly adsorbed in the sinusoidal channel, while at 773 K, adsorption in the super cage is favored for entropic reasons. (Thumbnails of the cluster model are shown to indicate the viewing angle used to create the heat maps. Framework atoms outside the plane represented in the heat maps have been omitted for clarity.) The color scale represents the percentage of configurations in which the C atom is found in a square area of 0.05 $Å^2$.

3 Results and Discussion

3.1 Influence of the zeolite structure on activation enthalpies and entropies of n-butane cracking and dehydrogenation

Figures 5-8 show experimental[10] as well as calculated apparent and intrinsic activation enthalpies and entropies for central cracking (Figure 5), terminal cracking (Figure 6), methylene dehydrogenation (Figure 7) and methyl dehydrogenation (Figure 8) of n-butane at 773 K in the zeolite frameworks of interest. In these figures, apparent parameters ($\Delta H^{\ddagger}_{app}$ and $\Delta S^{\ddagger}_{app}$) are shown in panels a and b, and their intrinsic counterparts ($\Delta H^{\ddagger}_{int}$ and $\Delta S^{\ddagger}_{int}$) are given in panels c and d. As in ref. 10, each set of activation parameters is plotted versus the Boltzmann-average values of $\Delta S_{ads\text{-}H+}$ (calculated using CBMC simulations). The value of $\Delta S_{ads\text{-}H+}$ serves as a proxy for the average level of confinement of n-butane within a given zeolite framework having a random distribution of Al atoms, with more negative values corresponding in general to more confining pore environments.[10] It is important to note that confinement is a geometric concept that depends on the structural details of the framework, and could only be fully characterized by $\Delta S_{ads\text{-}H+}$ in a perfectly homologous series of zeolites. A detailed discussion of the correlation between confinement, zeolite topology and suitable thermodynamic descriptors is given in ref. 66.

3.1.1 Central cracking

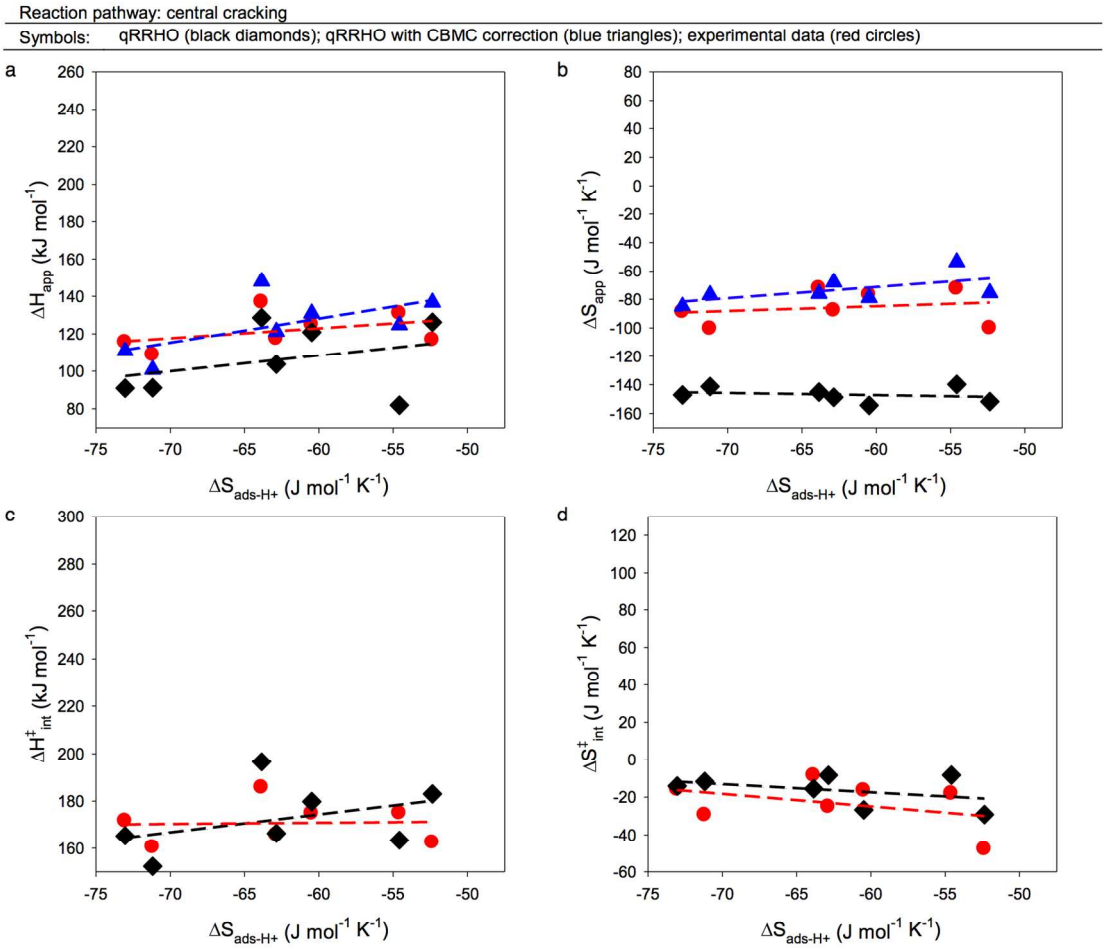

Figure 5. Plots of apparent activation enthalpy (a) and entropy (b), and intrinsic activation enthalpy (c) and entropy (d) vs. adsorption entropy determined from CBMC simulations[10] for central cracking of n-butane at 773 K. Experimental values reported by Janda et al.[10] (red circles) are compared with theoretical values determined from QM/MM using the quasi-RRHO approach before (black diamonds) and after (blue triangles) adding the thermal corrections derived from CBMC simulations. Representative 95% confidence intervals for the experimental values of $\Delta H^{\ddagger}_{app}$ and $\Delta S^{\ddagger}_{app}$ are ±7 kJ mol^{-1} and ±9 J mol^{-1} K^{-1}.[10]

The intrinsic and apparent enthalpies of activation for central cracking calculated using QM/MM (Figure 5, panel a and c) are in reasonably good agreement with the experimental values for all seven zeolites except $\Delta H^{\ddagger}_{app}$ for MWW. As noted in ref. 10, the uncertainty of individual experimental data points depends on the slope and the quality of the fit of the data to the Arrhenius equation. Representative 95% confidence intervals are ±7 kJ mol^{-1} for activation

enthalpies and ±9 J mol^{-1} K^{-1} for activation entropies.[10] Using the quasi-RRHO approach alone, $\Delta H^{\ddagger}_{app}$ for MWW is underestimated by 49 kJ mol^{-1}. After adding $\Delta\Delta H_{config}$, however, this difference is reduced to 15 kJ mol^{-1}, bringing the data point for MWW in line with the points for the other frameworks. The agreement of theory with experiment also improves or is nearly unchanged for the remaining frameworks upon applying the CBMC corrections to $\Delta H^{\ddagger}_{app}$. The large magnitude of the correction for MWW is consistent with the large size of the super cage (which is the largest cage structure present in all zeolites investigated)[10] and with the diffuse nature of the reactant-state configurations at 773 K (cf. Figure 4). The values of $\Delta H^{\ddagger}_{app}$ and $\Delta H^{\ddagger}_{int}$, determined from experiments as well as from the theoretical calculations, do not exhibit a significant correlation with $\Delta S_{ads\text{-}H+}$. These observations are consistent with the early character of the central cracking TS,[20] in which the substrate is tightly bound to the active site, and is therefore expected to be relatively insensitive to the size and geometry of the zeolite cavity.

Experimental and calculated apparent and intrinsic entropies of activation for central cracking are shown in panels b and d of Figure 5. While intrinsic activation entropies from theory and experiment are in reasonable agreement, apparent entropy changes calculated using the quasi-RRHO approach underestimate the experimental values by 41-77 J mol^{-1} K^{-1} depending on the framework. This discrepancy appears to result from the global motions of the transition state, which are not accounted for in the QM/MM calculations, since adding $\Delta\Delta S_{config}$ to $\Delta S^{\ddagger}_{app}$ improves the agreement significantly for all zeolites, again leaving no clear trend between the remaining discrepancies and the framework type. The value of $\Delta\Delta S_{config}$ ranges from 62 to 89 J mol^{-1} K^{-1}, with the lower values corresponding to the most confining zeolite topologies (TON, FER and -SVR) because as the size of the zeolite cavity increases, adsorbed alkanes have greater freedom to rotate and translate. Consequently, the configurational entropy unaccounted for by

the quasi-RRHO approach is correspondingly larger. In the more confining zeolite frameworks, both the reactant and the TS are less free to translate or rotate, and therefore entropy contributions from these modes are closer in magnitude to the vibrational estimates.

3.1.2 Terminal cracking

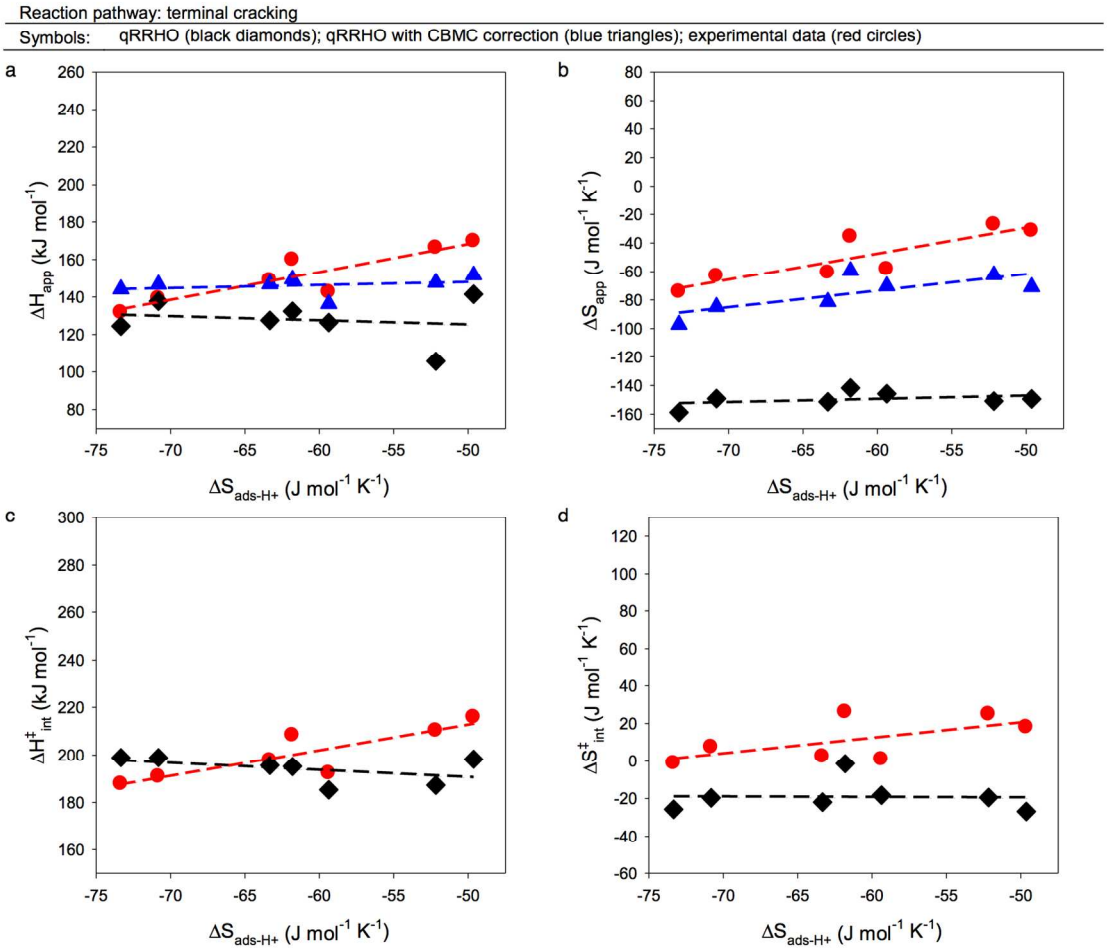

Figure 6. Plots of apparent activation enthalpy (a) and entropy (b), and intrinsic activation enthalpy (c) and entropy (d) vs. adsorption entropy determined from CBMC simulations[10] for terminal cracking of n-butane at 773 K. Experimental values reported by Janda et al.[10] (red circles) are compared with theoretical values determined from QM/MM using the quasi-RRHO approach, before (black diamonds) and after (blue triangles) adding the thermal corrections derived from CBMC simulations. Representative 95% confidence intervals for the experimental values of $\Delta H^{\ddagger}_{app}$ and $\Delta S^{\ddagger}_{app}$ are ±7 kJ mol^{-1} and ±9 J mol^{-1} K^{-1}.[10]

Apparent and intrinsic enthalpies and entropies of activation for terminal cracking are shown in Figure 6. The activation enthalpies for terminal cracking are higher relative to those for central cracking (Figure 5). Calculated values of $\Delta H^{\ddagger}_{int}$ and CBMC-corrected values of $\Delta H^{\ddagger}_{app}$ are generally in good agreement with experimentally observed values, especially considering the

representative uncertainty of +/- 7 kJ mol^{-1} on the latter, although the agreement is better for the more confining frameworks than for the two least confining frameworks, MWW and STF. In contrast to central cracking, the experimental enthalpies and entropies of activation show a slight upward trend going from more to less confining frameworks. This trend is not captured by the QM/MM values without the configurational correction term, resulting in an increasing deviation between theory and experiment with decreasing confinement. After adding the configurational corrections derived from CBMC, an upward trend in the apparent activation parameters with respect to $\Delta S_{ads\text{-}H+}$ can be seen that is qualitatively similar to that exhibited by the experimental data. This observation supports the validity of the assumption that the transition state for terminal cracking possesses similar rotational and translational entropy to that of the reactant state. The effect of adding the CBMC correctional terms to $\Delta H^{\ddagger}_{app}$ and $\Delta S^{\ddagger}_{app}$ is to account for such motions, and the entropy contributed by these modes increases with decreasing confinement.

However, despite the similar trends seen in the experimental and CBMC-corrected values of $\Delta H^{\ddagger}_{app}$ and $\Delta S^{\ddagger}_{app}$, calculated values of $\Delta S^{\ddagger}_{app}$ and (to a lesser extent) $\Delta H^{\ddagger}_{app}$ are systematically more negative than experimentally measured values, especially at lower confinement, which suggests that an additional source of entropy becomes increasingly important to the transition state at low confinement. The source of this entropy could be rotation of the ethyl group adjacent to the breaking C-C bond (cf. Figure 3), resulting in a more flexible TS with a larger conformational space for terminal cracking. The effect of this internal rotation is expected to be more prominent in the less confining frameworks.

3.1.3 Dehydrogenation

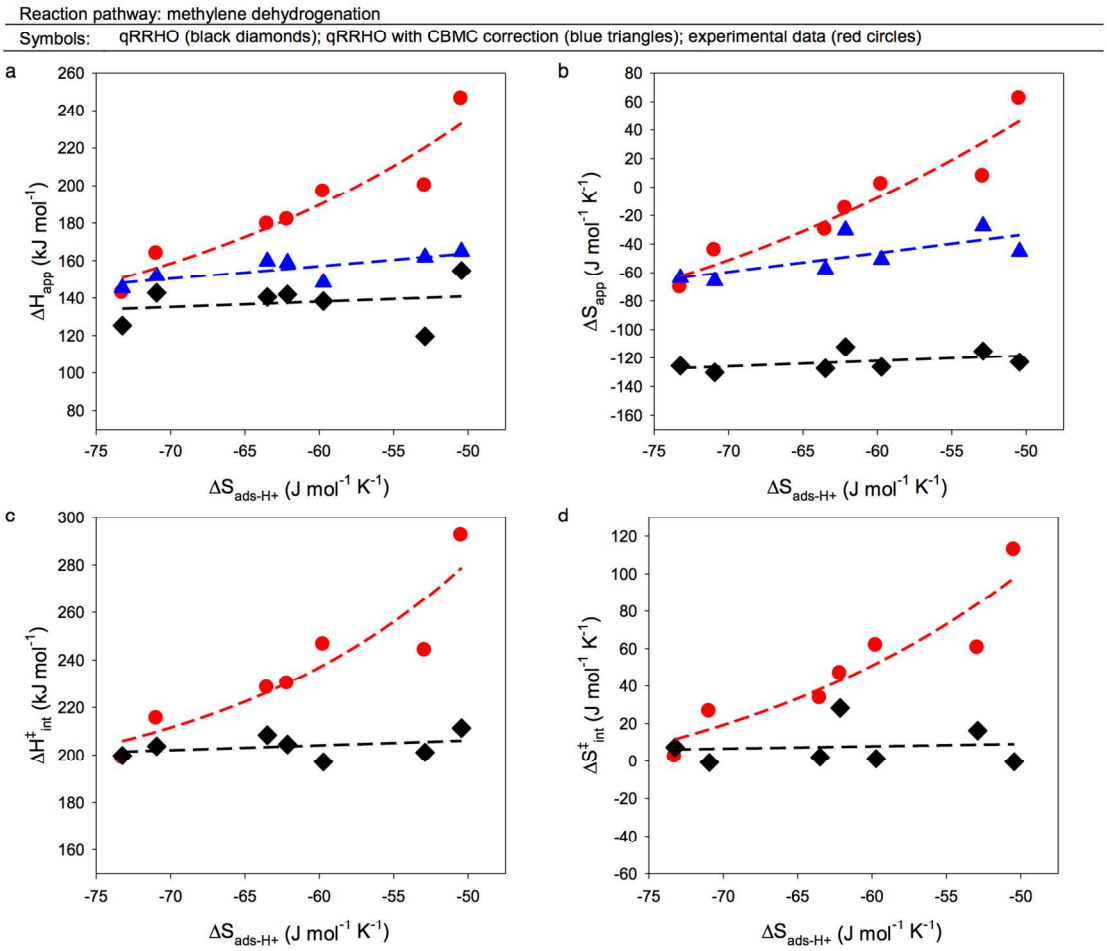

Figure 7. Plots of apparent activation enthalpy (a) and entropy (b), and intrinsic activation enthalpy (c) and entropy (d) vs. adsorption entropy determined from CBMC simulations[10] for methylene dehydrogenation of n-butane at 773 K. Experimental values reported by Janda et al.[10] (red circles) are compared with theoretical values determined from QM/MM using the quasi-RRHO approach, before (black diamonds) and after (blue triangles) adding the thermal corrections derived from CBMC simulations. Representative 95% confidence intervals for the experimental values of $\Delta H^{\ddagger}_{app}$ and $\Delta S^{\ddagger}_{app}$ are ±8 kJ mol^{-1} and ±11 J mol^{-1} K^{-1}.[10]

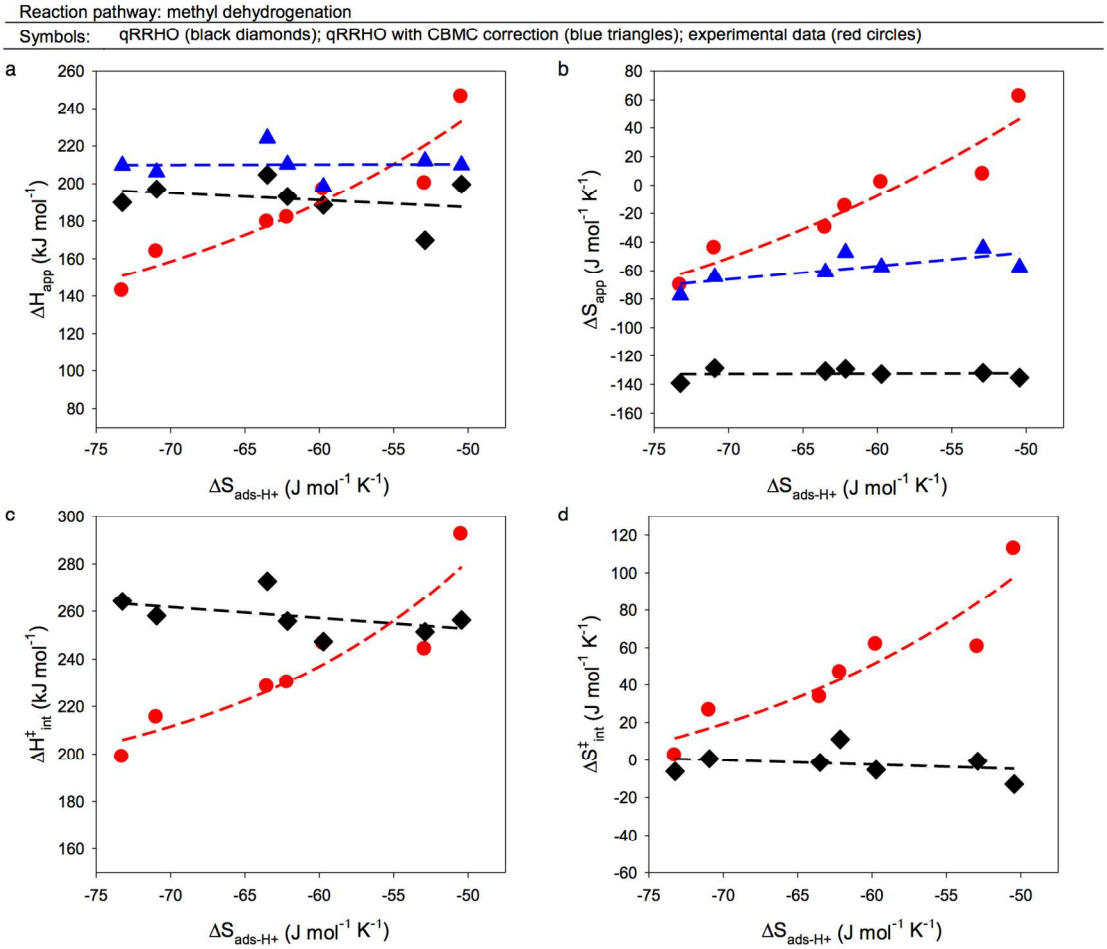

Figure 8. Plots of apparent activation enthalpy (a) and entropy (b), and intrinsic activation enthalpy (c) and entropy (d) vs. adsorption entropy determined from CBMC simulations[10] for methyl dehydrogenation of n-butane at 773 K. Experimental values reported by Janda et al.[10] (red circles) are compared with theoretical values determined from QM/MM using the quasi-RRHO approach, before (black dianonds) and after (blue triangles) adding the thermal corrections derived from CBMC. Representative 95% confidence intervals for the experimental values of $\Delta H^{\ddagger}_{app}$ and $\Delta S^{\ddagger}_{app}$ are ±8 kJ mol^{-1} and ±11 J mol^{-1} K^{-1}.[10]

Activation parameters corresponding to n-butane dehydrogenation via activation of methylene and methyl C-H bonds are presented in Figure 7 and Figure 8, respectively. Because butene undergoes rapid 1,2 isomerization at reaction temperatures, the contribution of methylene and methyl dehydrogenation pathways to the rate cannot be determined experimentally.

Therefore, computed activation parameters for both methylene dehydrogenation (Figure 7) and methyl dehydrogenation (Figure 8) must be compared with experimental values to gain mechanistic insights. However, the calculated values of $\Delta H^{\ddagger}_{app}$ are significantly higher for methyl C-H activation (Figure 8, panel a) than for methylene C-H activation (Figure 7, panel a), in line with the generally accepted stability order of the carbenium ions formed in the respective transition states (methyl C-H: primary carbenium ions; methylene C-H secondary carbenium ion – cf. Figure 3), while the calculated values of $\Delta S^{\ddagger}_{app}$ are similar for both pathways (panel b in Figures 7 and 8). Therefore, the methylene dehydrogenation pathway is expected to prevail in all frameworks, and further discussion is centered on a comparison of theory with experiment for methylene dehydrogenation (Figure 7).

Values of $\Delta H^{\ddagger}_{app}$ and $\Delta S^{\ddagger}_{app}$ calculated using the quasi-RRHO approach (black symbols) significantly underestimate the experimentally measured ones for all zeolite frameworks. For dehydrogenation, the experimentally observed increase in $\Delta H^{\ddagger}_{app}$ and $\Delta S^{\ddagger}_{app}$ with decreasing confinement is not properly recovered by the QM/MM calculations. When the configurational corrections derived from CBMC are added to the QM/MM values, better agreement is obtained between experiment and theory for $\Delta H^{\ddagger}_{app}$, and especially for $\Delta S^{\ddagger}_{app}$. An upward trend emerges in $\Delta H^{\ddagger}_{app}$ and $\Delta S^{\ddagger}_{app}$ with respect to $\Delta S_{ads\text{-}H+}$, albeit not as strong as that exhibited by the experimental values. Consequently, as confinement decreases, the discrepancy between experiment and theory increases more significantly than for terminal cracking. These deviations may be attributed to the later transition state for dehydrogenation compared to cracking.[20] For dehydrogenation, the H_2 product is virtually completely formed and is already moving away from the nascent butene (cf. Figure 3). Relative movements between the two fragments of the more disjointed TS remain unaccounted for by the CBMC corrections, which only reflect the

global mobility of the TS about the active site as derived from calculations of reactant adsorption. These relative motions become increasingly prominent in less confining frameworks, and would also affect $\Delta S^{\ddagger}_{int}$ and $\Delta H^{\ddagger}_{int}$, due to configurations of the TS with an increased charge separation. For both intrinsic parameters, an increasing deviation between theory and experiment is also observed with decreasing confinement. The magnitude of these deviations for $\Delta S^{\ddagger}_{int}$ are furthermore consistent with simplified statistical mechanics estimates of the entropy generated upon forming products of n-butane dehydrogenation within the MFI intersection.[34]

For reactions with increasingly loose transition states, especially in more open frameworks, the free energy bottlenecks separating reactants and products may be very different from the enthalpy bottlenecks identified by the saddle points optimized at 0 K.[67] Higher enthalpy configurations may become relevant due to favorable entropy, and a more rigorous description of the transition state based on molecular dynamics (MD) methods that allow sampling the complete free energy space at operational temperatures may be required. Accelerated sampling methods to simulate reactions with ab initio MD such as metadynamics,[68] combined with umbrella sampling,[69] and transition path sampling[70,71] have recently found application in zeolite catalysis. [3-5,50,72-78] While these powerful approaches are very promising, they come with a much higher computational cost. Furthermore, separating the obtained free energy barriers into individual enthalpy and entropy contributions is not straightforward and requires further investigation.

4 Conclusions

We have performed a theoretical study of the effects of zeolite topology on butane cracking and dehydrogenation to elucidate the experimentally observed variations in activation enthalpy and entropy for these reactions. We have leveraged a combination of CBMC simulations with QM/MM calculations employed in previous work to account for configurational enthalpy and entropy due to the mobility of the substrate within the zeolite cavity. Following this approach, we obtained apparent and intrinsic enthalpies and entropies of activation in good agreement with experiment for central cracking. For central cracking, which has an early transition state, $\Delta H^{\ddagger}_{app}$ and $\Delta S^{\ddagger}_{app}$ show no significant correlation with framework confinement. The corrections derived from CBMC successfully account for configurational enthalpy and entropy due to global motions of the transition state, resulting in good agreement of the apparent activation parameters between theory and experiment for all zeolites. For terminal cracking, experimental enthalpies and entropies of activation show an upward trend with decreasing confinement of the zeolite framework, which is not entirely captured by the calculations. Good agreement is still attained for the narrower pore topologies, but increasing deviations between theory and experiment emerge for the less confining zeolites, suggesting that an additional contribution of entropy to the transition state becomes increasingly important at low confinement. This effect is even more pronounced for dehydrogenation. While it is not possible to distinguish between methylene and methyl dehydrogenation experimentally, calculations indicate that the methylene pathway would prevail because its lower activation enthalpy is lower, and both pathways have a similar activation entropy. The experimentally observed increase in $\Delta H^{\ddagger}_{app}$ and $\Delta S^{\ddagger}_{app}$ with decreasing confinement is not fully reproduced by the calculations, even after including the corrections from CBMC. Because transition states for dehydrogenation occur later along the reaction coordinate

than for cracking, increased relative movements emerge between the saturated fragment expelled in the reaction (C_2H_6 in central cracking, CH_4 in terminal cracking, H_2 in dehydrogenation) and the remaining alkene, in addition to the global motions accounted for by the CBMC corrections. Such motions also affect $\Delta H^{\ddagger}_{int}$ and $\Delta S^{\ddagger}_{int}$, for which an increasing deviation between theory and experiment is also observed with decreasing confinement. These observations indicate that as transition states become increasingly loose, they can no longer be adequately characterized by single saddle points, especially in less confining zeolites, and more advanced sampling methods based on ab initio molecular dynamics will be necessary to correctly identify the free energy bottlenecks for these reactions.

5 Supporting Information

Additional details on the accessibility assessment of the T-sites selected for Al substitution, overview of critical distances in the transition states for butane cracking and dehydrogenation, additional details of the Mobile Block analysis performed on the reactant and transition states obtained from QM/MM.

6 Acknowledgements

This work was supported by Chevron Energy Technology. JVdM also acknowledges funding from the Ghent University Research Board (BOF). Computational resources were provided by the Ohio Supercomputer Center[79] and UC Berkeley's Molecular Graphics and Computation Facility (supported by NSF Grant CHE-0840505).

7 References

(1) Haag, W. O.; Dessau, R. M. *Proceedings − International Congress on Catalysis*, 8th, Berlin, Verlag Chemie: Weinheim, 1984; Vol. 2, pp 305−316.
(2) Kotrel, S.; Knözinger, H.; Gates, B. C. *Micro. Meso. Mater.* **2000**, *35-36*, 11–20.
(3) Bučko, T.; Benco, L.; Dubay, O.; Dellago, C.; Hafner, J. *J. Chem. Phys.* **2009**, *131*, 214508.
(4) Bučko, T.; Hafner, J. *J. Phys.: Condens. Matter* **2010**, *22*, 384201.
(5) Bučko, T.; Benco, L.; Hafner, J.; Ángyán, J. G. *J. Catal.* **2011**, *279*, 220–228.
(6) Zimmerman, P. M.; Tranca, D. C.; Gomes, J.; Lambrecht, D. S.; Head-Gordon, M.; Bell, A. T. *J. Am. Chem. Soc.* **2012**, *134*, 19468–19476.
(7) Konno, H.; Okamura, T.; Kawahara, T.; Nakasaka, Y.; Tago, T.; Masuda, T. *Chem. Eng. J.* **2012**, *207-208*, 490–496.
(8) Voogd, P.; Van Bekkum, H. *Appl. Catal.* **1990**, *59*, 311–331.
(9) Haag, W. O.; Lago, R. M.; Weisz, P. B. *Faraday Discuss. Chem. Soc.* **1981**, *72*, 317–330.
(10) Janda, A.; Vlaisavljevich, B.; Lin, L.-C.; Smit, B.; Bell, A. T. *J. Am. Chem. Soc.* **2016**, *138*, 4739–4756.
(11) Janda, A.; Vlaisavljevich, B.; Lin, L.-C.; Sharada, S. M.; Smit, B.; Head-Gordon, M.; Bell, A. T. *J. Phys. Chem. C* **2015**, *119*, 10427–10438.
(12) van Bokhoven, J. A.; Williams, B. A.; Ji, W.; Koningsberger, D. C.; Kung, H. H.; Miller, J. T. *J. Catal.* **2004**, *224*, 50–59.
(13) Gounder, R.; Iglesia, E. *J. Am. Chem. Soc.* **2009**, *131*, 1958–1971.
(14) Zheng, X.; Blowers, P. *J. Phys. Chem. A* **2005**, *109*, 10734–10741.
(15) Gounder, R.; Iglesia, E. *Acc. Chem. Res.* **2012**, *45*, 229–238.
(16) Ramachandran, C. E.; Williams, B. A.; van Bokhoven, J. A. *J. Catal.* **2005**, *233*, 100–108.
(17) van Bokhoven, J. A.; Xu, B. *Stud. Surf. Sci. Catal.* **2007**.
(18) Babitz, S. M.; Williams, B. A.; Miller, J. T.; Snurr, R. Q.; Haag, W. O.; Kung, H. H. *Appl. Catal. A Gen* **1999**, *179*, 71–86.
(19) Swisher, J. A.; Hansen, N.; Maesen, T.; Keil, F. J.; Smit, B.; Bell, A. T. *J. Phys. Chem. C* **2010**, *114*, 10229–10239.
(20) Sharada, S. M.; Zimmerman, P. M.; Bell, A. T.; Head-Gordon, M. *J. Phys. Chem. C* **2013**, *117*, 12600–12611.
(21) Zimmerman, P. M.; Head-Gordon, M.; Bell, A. T. *J. Chem. Theory Comput.* **2011**, *7*, 1695–1703.
(22) Maihom, T.; Pantu, P.; Tachakritikul, C.; Probst, M.; Limtrakul, J. *J. Phys. Chem. C* **2010**, *114*, 7850–7856.
(23) Tranca, D. C.; Hansen, N.; Swisher, J. A.; Smit, B.; Keil, F. J. *J. Phys. Chem. C* **2012**, *116*, 23408–23417.
(24) Ding, B. J.; Huang, S. P.; Wang, W. C. *Chin. J. Chem.* **2008**, *26*, 1173–1180.
(25) Zygmunt, S. A.; Curtiss, L. A.; Zapol, P.; Iton, L. E. *J. Phys. Chem. B* **2000**, *104*, 1944–1949.
(26) Frash, M. V.; van Santen, R. A. *Top. Catal.* **1999**, *9*, 191–205.
(27) Rigby, A. M.; Kramer, G. J.; van Santen, R. A. *J. Catal.* **1997**, *170*, 1–10.
(28) Kazansky, V. B.; Frash, M. V.; van Santen, R. A. *Appl. Catal. A Gen.* **1996**, *146*, 225–

247.
(29) Blaszkowski, S. R.; Nascimento, M. A. C.; van Santen, R. A. *J. Phys. Chem.* **1996**, *100*, 3463–3472.
(30) Collins, S. J.; O'Malley, P. J. *Chem. Phys. Lett.* **1995**, *246*, 555–561.
(31) Collins, S. J.; Omalley, P. J. *J. Catal.* **1995**, *153*, 94–99.
(32) Bučko, T. *J. Phys.: Condens. Matter* **2008**, *20*, 064211.
(33) Grimme, S. *Chemistry* **2012**, *18*, 9955–9964.
(34) Janda, A.; Bell, A. T. *J. Am. Chem. Soc.* **2013**, *135*, 19193–19207.
(35) Structure Commission of the International Zeolite Association. http://www.iza-structure.org/databases/.
(36) Dědeček, J.; Sobalík, Z.; Wichterlová, B. *Catal. Rev.* **2012**, *54*, 135–223.
(37) First, E. L.; Gounaris, C. E.; Wei, J.; Floudas, C. A. *Phys. Chem. Chem. Phys.* **2011**, *13*, 17339–17358.
(38) Sklenak, S.; Dědeček, J.; Li, C.; Gao, F.; Jansang, B.; Boekfa, B.; Wichterlová, B.; Sauer, J. *Collect. Czech. Chem. Commun.* **2008**, *73*, 909–920.
(39) Baerlocher, C.; Xie, D.; McCusker, L. B.; Hwang, S.-J.; Chan, I. Y.; Ong, K.; Burton, A. W.; Zones, S. I. *Nat. Mater.* **2008**, *7*, 631–635.
(40) Bushuev, Y. G.; Sastre, G. *J. Phys. Chem. C* **2009**, *113*, 10877–10886.
(41) Gomes, J.; Zimmerman, P. M.; Head-Gordon, M.; Bell, A. T. *J. Phys. Chem. C* **2012**, *116*, 15406–15414.
(42) Van Speybroeck, V.; Van der Mynsbrugge, J.; Vandichel, M.; Hemelsoet, K.; Lesthaeghe, D.; Ghysels, A.; Marin, G. B.; Waroquier, M. *J. Am. Chem. Soc.* **2011**, *133*, 888–899.
(43) Van der Mynsbrugge, J.; Hemelsoet, K.; Vandichel, M.; Waroquier, M.; Van Speybroeck, V. *J. Phys. Chem. C* **2012**, *116*, 5499–5508.
(44) Van der Mynsbrugge, J.; Visur, M.; Olsbye, U.; Beato, P.; Bjørgen, M.; Van Speybroeck, V.; Svelle, S. *J. Catal.* **2012**, *292*, 201–212.
(45) Kokotailo, G. T.; Chu, P.; Lawton, S. L.; Meier, W. M. *Nature* **1978**, *275*, 119–120.
(46) Paul Wagner; Yumi Nakagawa; Greg S Lee; Mark E Davis; Saleh Elomari; Ronald C Medrud, A.; S I Zones. *J. Am. Chem. Soc.* **1999**, *122*, 263–273.
(47) Leonowicz, M. E.; Lawton, J. A.; Lawton, S. L.; Rubin, M. K. *Science* **1994**, *264*, 1910–1913.
(48) Zhou, D.; Bao, Y.; Yang, M.; He, N.; Yang, G. *J. Mol. Catal. A Chem.* **2006**, *244*, 11–19.
(49) Li, Y.; Guo, W.; Fan, W.; Yuan, S.; Li, J.; Wang, J.; Jiao, H.; Tatsumi, T. *J. Mol. Catal. A Chem.* **2011**, *338*, 24–32.
(50) Bučko, T.; Hafner, J. *J. Catal.* **2015**, *329*, 32–48.
(51) Li, Y.-P.; Gomes, J.; Mallikarjun Sharada, S.; Bell, A. T.; Head-Gordon, M. *J. Phys. Chem. C* **2015**, *119*, 1840–1850.
(52) Shao, Y.; Molnar, L. F.; Jung, Y.; Kussmann, J.; Ochsenfeld, C.; Brown, S. T.; Gilbert, A. T. B.; Slipchenko, L. V.; Levchenko, S. V.; O'Neill, D. P.; DiStasio, R. A., Jr; Lochan, R. C.; Wang, T.; Beran, G. J. O.; Besley, N. A.; Herbert, J. M.; Lin, C. Y.; Van Voorhis, T.; Chien, S. H.; Sodt, A.; Steele, R. P.; Rassolov, V. A.; Maslen, P. E.; Korambath, P. P.; Adamson, R. D.; Austin, B.; Baker, J.; Byrd, E. F. C.; Dachsel, H.; Doerksen, R. J.; Dreuw, A.; Dunietz, B. D.; Dutoi, A. D.; Furlani, T. R.; Gwaltney, S. R.; Heyden, A.; Hirata, S.; Hsu, C.-P.; Kedziora, G.; Khalliulin, R. Z.; Klunzinger, P.;

Lee, A. M.; Lee, M. S.; Liang, W.; Lotan, I.; Nair, N.; Peters, B.; Proynov, E. I.; Pieniazek, P. A.; Rhee, Y. M.; Ritchie, J.; Rosta, E.; Sherrill, C. D.; Simmonett, A. C.; Subotnik, J. E.; Woodcock, H. L., III; Zhang, W.; Bell, A. T.; Chakraborty, A. K.; Chipman, D. M.; Keil, F. J.; Warshel, A.; Hehre, W. J.; Schaefer, H. F., III; Kong, J.; Krylov, A. I.; Gill, P. M. W.; Head-Gordon, M. *Phys. Chem. Chem. Phys.* **2006**, *8*, 3172–3191.

(53) Verstraelen, T.; Van Speybroeck, V.; Waroquier, M. *J. Chem. Inf. Model.* **2008**, *48*, 1530–1541.

(54) Chai, J.-D.; Head-Gordon, M. *J. Chem. Phys.* **2008**, *128*, 084106.

(55) Chai, J.-D.; Head-Gordon, M. *Phys. Chem. Chem. Phys.* **2008**, *10*, 6615–6620.

(56) Foloppe, N.; MacKerell, A. D., Jr. *J. Comput. Chem.* **2000**, *21*, 86–104.

(57) Yin, D.; MacKerell, A. D. *J. Comput. Chem.* **1998**, *19*, 334–348.

(58) Vanommeslaeghe, K.; Hatcher, E.; Acharya, C.; Kundu, S.; Zhong, S.; Shim, J.; Darian, E.; Guvench, O.; Lopes, P.; Vorobyov, I.; Mackerell, A. D. *J. Comput. Chem.* **2010**, *31*, 671–690.

(59) Behn, A.; Zimmerman, P. M.; Bell, A. T.; Head-Gordon, M. *J. Chem. Phys.* **2011**, *135*, 224108.

(60) Baker, J. *J. Comput. Chem.* **1986**, *7*, 385–395.

(61) De Moor, B. A.; Reyniers, M.-F.; Marin, G. B. *Phys. Chem. Chem. Phys.* **2009**, *11*, 2939–22.

(62) De Moor, B. A.; Reyniers, M.-F.; Gobin, O. C.; Lercher, J. A.; Marin, G. B. *J. Phys. Chem. C* **2011**, *115*, 1204–1219.

(63) De Moor, B. A.; Ghysels, A.; Reyniers, M.-F.; Van Speybroeck, V.; Waroquier, M.; Marin, G. B. *J. Chem. Theory Comput.* **2011**, *7*, 1090–1101.

(64) Ghysels, A.; Van Neck, D.; Van Speybroeck, V.; Verstraelen, T.; Waroquier, M. *J. Chem. Phys.* **2007**, *126*, 224102.

(65) Ghysels, A.; Verstraelen, T.; Hemelsoet, K.; Waroquier, M.; Van Speybroeck, V. *J. Chem. Inf. Model.* **2010**, *50*, 1736–1750.

(66) Janda, A.; Vlaisavljevich, B.; Smit, B.; Lin, L.-C.; Bell, A. T. *J. Phys. Chem. C* **2017**, *121*, 1618–1638.

(67) Gomes, J.; Head-Gordon, M.; Bell, A. T. *J. Phys. Chem. C* **2014**, *118*, 21409–21419.

(68) Laio, A.; Parrinello, M. *Proc. Nat. Acad. Sci.* **2002**, *99*, 12562–12566.

(69) Ensing, B.; Laio, A.; Parrinello, M.; Klein, M. L. *J. Phys. Chem. B* **2005**, *109*, 6676–6687.

(70) Dellago, C.; Bolhuis, P. G.; Geissler, P. L. *Transition Path Sampling*; John Wiley & Sons, Inc.: Hoboken, NJ, USA, 2002; Vol. 123, pp 1–78.

(71) Bolhuis, P. G.; Chandler, D.; Dellago, C.; Geissler, P. L. *Annu. Rev. Phys. Chem.* **2002**, *53*, 291–318.

(72) Moors, S. L. C.; De Wispelaere, K.; Van der Mynsbrugge, J.; Waroquier, M.; Van Speybroeck, V. *ACS Catal.* **2013**, *3*, 2556–2567.

(73) Van der Mynsbrugge, J.; Moors, S. L. C.; De Wispelaere, K.; Van Speybroeck, V. *ChemCatChem* **2014**, *6*, 1906–1918.

(74) De Wispelaere, K.; Ensing, B.; Ghysels, A.; Meijer, E. J.; Van Speybroeck, V. *Chem. Eur. J.* **2015**, *21*, 9385–9396.

(75) Van Speybroeck, V.; De Wispelaere, K.; Van der Mynsbrugge, J.; Vandichel, M.; Hemelsoet, K.; Waroquier, M. *Chem. Soc. Rev.* **2014**, *43*, 7326–7357.

(76) Van Speybroeck, V.; Hemelsoet, K.; Joos, L.; Waroquier, M.; Bell, R. G.; Catlow, C. R. A. *Chem. Soc. Rev.* **2015**, *44*, 7044–7111.
(77) Hajek, J.; Van der Mynsbrugge, J.; De Wispelaere, K.; Cnudde, P.; Vanduyfhuys, L.; Waroquier, M.; Van Speybroeck, V. *J. Catal.* **2016**, *340*, 227–235.
(78) Cnudde, P.; De Wispelaere, K.; Van der Mynsbrugge, J.; Waroquier, M.; Van Speybroeck, V. *J. Catal.* **2017**, *345*, 53–69.
(79) Ohio Supercomputer Center, http://osc.edu/ark:/19495/f5s1ph73, 1987.

TOC Graphic

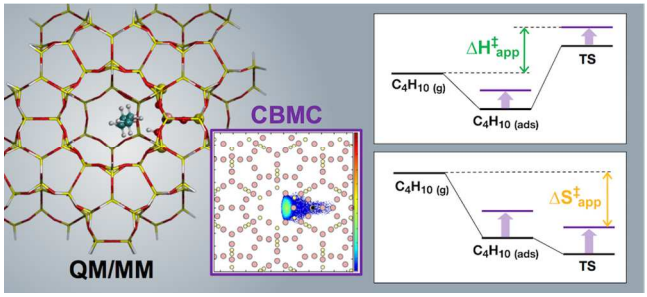
CBMC
QM/MM
$\Delta H^{\ddagger}_{app}$
TS
C_4H_{10} (g)
C_4H_{10} (ads)
C_4H_{10} (g)
$\Delta S^{\ddagger}_{app}$
C_4H_{10} (ads)
TS